

Thermophysical properties of gases, liquids, and solids composed of particles interacting with a short-range attractive potential

Siegfried Hess¹ and Martin Kröger^{1,2}¹*Institut für Theoretische Physik, Technische Universität Berlin, PN 7-1, Hardenbergstrasse 36, D-10623 Berlin, Germany*²*Polymerphysik, Institut für Polymere, ETH Zürich, Sonneggstrasse 3, CH-8092 Zürich, Switzerland*

(Received 23 December 2000; revised manuscript received 28 February 2001; published 8 June 2001)

A short-range polynomial interaction potential is introduced which has both a repulsive core and an attractive part. It is cut off smoothly such that its first and second derivatives vanish at the cutoff distance. The potential therefore enables efficient simulation studies of a model material that exhibits similarities to a full (but computationally expensive) classical Lennard-Jones system. Thermophysical properties of the model are calculated by (nonequilibrium) molecular dynamics computer simulations and compared with analytical results. Among the quantities studied is the pressure as a function of the density for various temperatures. Equations of state for the fluid and the solid are tested. The coexistence of gaseous, (metastable) liquid, and fcc solid phases is found for a range of temperatures. Bulk and shear moduli are computed. The response of the system to a shear deformation with a constant shear rate is analyzed. The liquid shows viscoelastic behavior that can be described with a Maxwell model. The solid behaves as an elastic medium up to a finite deformation and then undergoes a transition to plastic flow, which is stick-slip-like at small shear rates and continuous at higher ones.

DOI: 10.1103/PhysRevE.64.011201

PACS number(s): 83.50.-v, 47.10.+g, 64.10.+h, 46.35.+z

I. INTRODUCTION

Statistical physics aims to explain the thermophysical properties of matter and dynamic phenomena occurring in nonequilibrium processes on the basis of the properties of atoms and molecules and their interactions. Molecular dynamics (MD) and Monte Carlo computer simulations performed during recent decades have helped enormously to achieve this goal. The study of models plays an important role. Simple systems composed of (effectively) spherical particles are modeled with potentials that are linear combinations of the inverse power of the distance r between two particles. Both the repulsion at short distances and the attraction at larger distances are described in this way. The distance where the potential vanishes defines a characteristic length, the “diameter” r_0 of a particle. Such potentials were already used almost a century ago [1]; they are commonly referred to as Lennard-Jones (LJ) potentials [2]. In computer simulations, these potentials are usually cut off at a finite distance h , e.g., $h = 2.5r_0$ was popular for some time. Shorter cutoff distances are preferred in many nonequilibrium molecular dynamics (NEMD) simulations. The potential has to be shifted such that it vanishes at $r = h$ and, for MD simulations, it is desirable that the force also vanishes at the cutoff distance. A case favored in many numerical studies is a cutoff at the minimum, often referred to as the (purely repulsive) WCA potential [3]. Other amendments of the LJ potential have been proposed, e.g., the LJ potential is used until its point of inflection, and beyond this point it is replaced by a third order spline function such that the potential and its first derivative are continuous [4]. When one does not aim to mimic a particular substance, but just intends to catch certain essential features of the thermophysical behavior within a restricted temperature range, one may use alternative functional forms for the potential with an even smoother cutoff

[5]. Of course others have previously noticed the necessity for a smooth cutoff, e.g., Hoover and Posch [6], who used the potential $[1 - (r/r_0)^2]^4$, which, however, is rather different from the LJ potential and has a vanishing force for r going to zero.

Recently, it has been demonstrated that the density dependence of the energy and the pressure of the WCA fluid and fcc solid are reproduced by a short-range repulsive polynomial potential [7]. The smooth cutoff, where the second derivative of the potential is also continuous, is not only advantageous for the integration of the equations of motion, in particular for systems in nonequilibrium and with strong gradients as in shock waves. It is essential for the computation of elasticity coefficients in the solid phase since the microscopic expressions for the elasticity coefficients involve the second derivative of the potential. The same applies for the computation of the configurational temperature [8]. Here, a smoothly cut-off simple polynomial function is used that has a repulsive and a relatively short-range attractive (SHRAT) part ($h = 1.5r_0$). Properties of the model system in its gaseous, (metastable) liquid, and solid states are computed by MD and NEMD simulations and, where possible, compared with analytical calculations, as well as with the behavior of real substances.

The thermophysical properties presented are the pressure as a function of the density at various temperatures, elasticity coefficients, non-Newtonian shear viscosity, and viscoelastic behavior of the liquid, as well as the elastic behavior under shear and the transition to plastic flow in the solid.

II. THE POTENTIAL CURVES

The 6-12 Lennard-Jones reference potential reads $\phi^{\text{LJ}}(r) = 4\Phi_0[(r/r_0)^{-12} - (r/r_0)^{-6}]$. The quantities Φ_0 and r_0 set the characteristic energy and length scales. The SHRAT potential to be used here is of the form $\phi^{\text{SHRAT}}(r)$

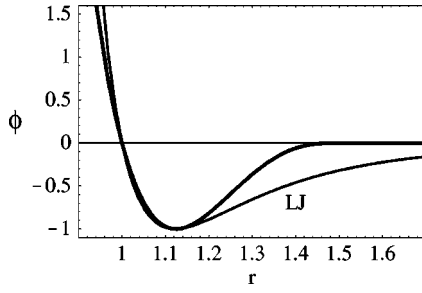


FIG. 1. The short-range attractive potential (SHRAT) function (thick curve) and the Lennard-Jones (LJ) potential (thinner curve) as functions of the distance r . All physical quantities are in standard LJ units.

$\sim 3(h-r)^4 - 4(h-r_{\min})(h-r)^3$ for $r \leq h$ and $\phi^{\text{SHRAT}}(r) = 0$ for $r > h$. This function has a minimum at $r = r_{\min}$. Its intersection with the horizontal axis is $r_0 = (4/3)r_{\min} - (1/3)h$. This functional form has been recently used for the effective two-particle interaction in a variant of the embedded atom method for metals [9,10].

If one requires, as in [5], that the force at $r = r_0$ and the depth of the potential at $r = r_{\min}$ be equal to the corresponding LJ values, one finds $h = (113/81)r_0 \approx 1.4r_0$ and $r_{\min} = (89/81)r_0 \approx 1.1r_0$. The resulting potential is $24\Phi_0(1 - r/r_0)[(h-r)/(h-r_{\min})]^3$. Here we choose the similar values $h = (3/2)r_0$, $r_{\min} = (9/8)r_0$ and set the depth of the potential equal to Φ_0 , in analogy with the LJ potential. The explicit expression for our model potential therefore reads

$$\phi^{\text{SHRAT}}(r) = \frac{512}{27}\Phi_0\left(1 - \frac{r}{r_0}\right)\left(3 - 2\frac{r}{r_0}\right)^3, \quad r \leq 1.5r_0, \quad (1)$$

and $\phi^{\text{SHRAT}}(r) = 0$ for $r > 1.5r_0$. In units of Φ_0/r_0 , the force at $r = r_0$ is $512/27 \approx 19$. The corresponding value for the LJ potential is 24. Notice that this potential is finite at $r = 0$, viz, $\phi^{\text{SHRAT}}(0) = 512\Phi_0$. For temperatures below $10\Phi_0/k_B$, this is of no practical concern since the Boltzmann factor $\exp(-\Phi_0/k_B T)$ governing the fraction of particles that can reach this distance is smaller than 6×10^{-23} .

In Fig. 1 the short-range potential used here and the LJ potential are plotted as functions of the distance r . In numerical calculations and in the graphs displayed here, all physical quantities are expressed in the standard LJ units of [11–14], e.g., lengths and energies are given in units of r_0 and Φ_0 . Following common practice the dimensionless variables are denoted by the same symbols as the corresponding physical quantities when no danger of confusion exists.

In dimensionless notation, the LJ and SHRAT potentials read $\phi^{\text{LJ}}(r) = 4(r^{-12} - r^{-6})$ and $\phi^{\text{SHRAT}}(r) = (512/27)(1 - r)(3 - 2r)^3$, $r \leq 3/2$, whereas $\phi^{\text{SHRAT}}(r) = 0$ for $r > 3/2$. Similarly, the number density $n = N/V$, where N and V are the number of particles and the volume of the system, and the temperature T are expressed in units of $n_{\text{ref}} = r_0^{-3}$ and $T_{\text{ref}} = \Phi_0/k_B$, respectively. The unit for the pressure is $p_{\text{ref}} = \Phi_0 r_0^{-3}$.

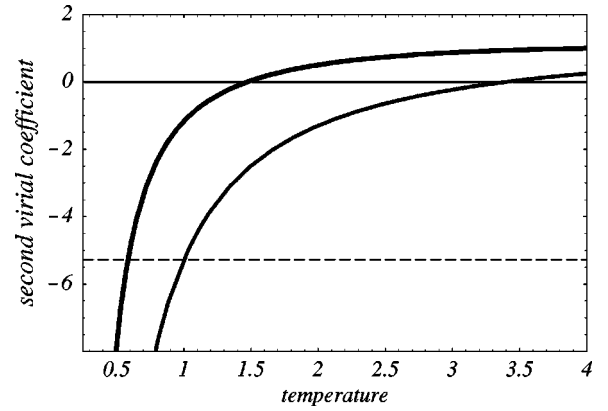


FIG. 2. The second virial coefficient pertaining to the SHRAT potential (thick curve) and to the LJ potential (thinner curve) as functions of the temperature T . All physical quantities are in standard LJ units.

III. PRESSURE VERSUS DENSITY

A. Dilute gas and ideal solid

Simple analytic expressions for the pressure are available, both for low density gases and for ideal solids. The pressure of a dilute gas, just one power in the density beyond the ideal gas, is given by $p = nk_B T [1 + nB_2(T)]$ with the second virial coefficient (per particle) $B_2(T)$. In Fig. 2 the second virial coefficient, in units of r_0^3 , is displayed as a function of the temperature for the SHRAT (upper, thicker curve) and for the LJ (lower, thinner curve) potentials. For spherical particles, the second virial coefficient is computed according to

$$B_2(T) = 2\pi \int_0^\infty \{1 - \exp[-\phi(r)/k_B T]\} r^2 dr. \quad (2)$$

In the calculation, the LJ potential is cut off at $r = 8r_0$. The dashed horizontal line marks the value $B_2^{\text{LJ}}(1)$. In the SHRAT case, this value is reached at $T/T_{\text{ref}} \approx 0.6$.

In the limit of low temperatures, one may assume that the particles occupy ideal lattice sites. Then one calculates the “cold” energy per particle $e = e_{\text{cold}}$ and the “cold” pressure $p = p_{\text{cold}}$ by inserting the density dependent nearest neighbor distance $a_{\text{fcc}} = (\sqrt{2}/2)(4/n)^{1/3}r_0$ for a close packed cubic (or hexagonal) solid into the two-particle energy and the virial, summed over the 12 nearest neighbors, when the density does not exceed $32/27 \approx 1.185$. Then one has, $e_{\text{cold}}(n) = 6\phi(a_{\text{fcc}}(n))$, and $p_{\text{cold}}(n) = n^2 \partial e_{\text{cold}} / \partial n = -2na_{\text{fcc}}(n)\phi'(a_{\text{fcc}}(n))$. Here ϕ and ϕ' stand for the SHRAT potential and its derivative with respect to the distance. For higher densities, the contributions from the next coordination shells have to be taken into account. The resulting curves are displayed in Fig. 3. The dashed curves show the corresponding results for particles placed on body centered cubic (bcc) lattice sites, where the nearest neighbor distance is linked with the density by $a_{\text{bcc}} = (\sqrt{3}/2) \times (2/n)^{1/3}r_0$. In that case, the eight first and the six second nearest neighbors have to be taken into account for densities less than $32\sqrt{2}/27 \approx 1.676$. Clearly, for densities close to

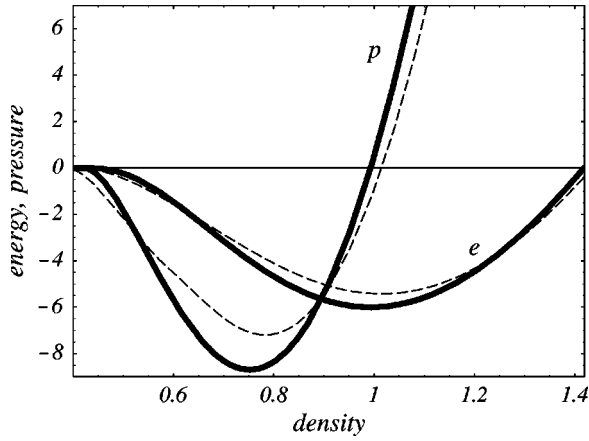


FIG. 3. The cold energy e (per particle) and pressure p as functions of the density for ideal fcc (solid curves) and bcc (dashed curves) solids. All physical quantities are in standard LJ units.

$n/n_{\text{ref}}=1$, the minimal energy is lower in the fcc solid. The fcc energy minimum $e = -6\Phi_0$ occurs at the density $n/n_{\text{ref}} = 4/(9\sqrt{2/8})^3 \approx 0.993$.

B. Remarks on MD simulations

Simulations at the constant temperatures $T/T_{\text{ref}} = 0.01, 0.1, 0.4, 0.6, 0.8, 1.0, 2.0$ and constant number densities $n = N/V$ (NVT ensemble simulations) in the range $n/n_{\text{ref}} = 0.1, \dots, 1.1$ were performed for $N = 4 \times 8^3 = 2048$ particles, where the initial positions were fcc lattice sites. The equations of motion were integrated with the velocity Verlet algorithm with the time step $\delta t/t_{\text{ref}} = 0.005$. The LJ reference time is $t_{\text{ref}} = r_0(m/\Phi_0)^{1/2}$, and m is the mass of a particle. A cubic simulation box with volume V and periodic boundary conditions were used. The temperature was kept constant by rescaling the magnitude of the particle velocities, which corresponds to the Gaussian constraint of constant kinetic energy. Typically, the system was aged for 2000 or more time steps corresponding to 10 or more reduced time units before the data were extracted as time averages over 4000 or more time steps corresponding to 20 or more time units. Due to a link list procedure [15], the computational time increases linearly with the number of particles N when $N > 500$.

The pressure $p = nk_B T + p^{\text{pot}}$ is the sum of the ‘‘kinetic’’ or ‘‘ideal gas’’ contribution $nk_B T$ and the ‘‘potential’’ contribution p^{pot} . The latter quantity is computed according to

$$V p^{\text{pot}} = \frac{1}{3} \left\langle \sum_i \mathbf{r}^i \cdot \mathbf{F}^i \right\rangle = \frac{1}{3} \left\langle \sum_{i < j} \mathbf{r}^{ij} \cdot \mathbf{F}^{ij} \right\rangle. \quad (3)$$

The angular brackets indicate a time average. Here $\mathbf{F}^i = \sum_{j \neq i} \mathbf{F}^{ij}$ is the force acting on particle i , $\mathbf{F}^{ij} = \mathbf{F}(\mathbf{r}^{ij})$ is the force exerted on particle i from particle j , and $\mathbf{F}(\mathbf{r}) = -\partial \phi(\mathbf{r})/\partial \mathbf{r}$. The symbol $\sum_{i < j}$ means a double summation over pairs of particles, with i less than j .

C. Pressure in the fluid and solid states

In the four graphs of Fig. 4 the symbols mark the computed pressures for given densities (via MD) for the tempera-

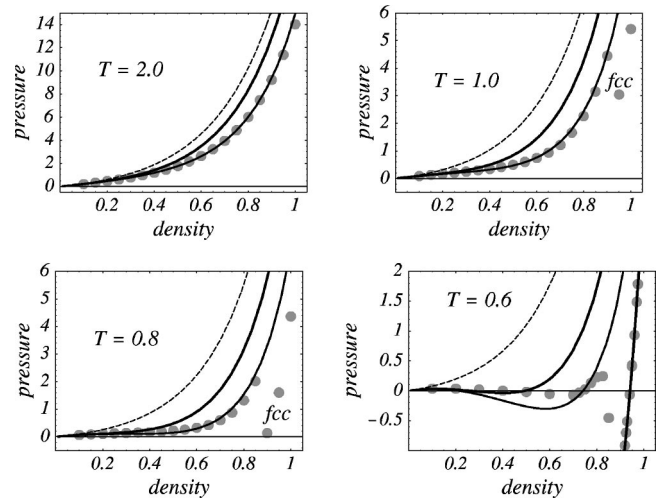


FIG. 4. The pressure as a function of the density for the temperatures $T/T_{\text{ref}} = 0.6, 0.8, 1.0, 2.0$. The dots indicate the results from the MD calculation. Except for the points at high densities, marked ‘‘fcc’’ for $T/T_{\text{ref}} = 1.0, 0.8$ and joined by a thick curve for $T/T_{\text{ref}} = 0.6$, the MD data pertain to the fluid, gaseous, or liquid state of the system. The curves stem from theoretical expressions explained in the text. All physical quantities are in standard LJ units.

tures $T/T_{\text{ref}} = 2.0, 1.0, 0.8, 0.6$ (from top left to bottom right). Most data points pertain to the fluid, gaseous, or liquid state of the system. Data at higher densities for the temperatures $T/T_{\text{ref}} = 1.0, 0.8, 0.6$ are for the fcc solid. At $T/T_{\text{ref}} = 2.0$ a fluid state exists only in the density range shown. On the other hand, at $T/T_{\text{ref}} = 0.6$, gaseous, liquid, and solid states exist at small, intermediate, and higher densities.

For the lower temperatures $T/T_{\text{ref}} = 0.6, 0.4, 0.1, 0.01$ the pressure of the fcc solid, as a function of the density, is displayed in Fig. 5. Negative values of the pressure, although indicating a mechanically unstable state, reveal that the liquid, and even more the solid, can withstand some tension due

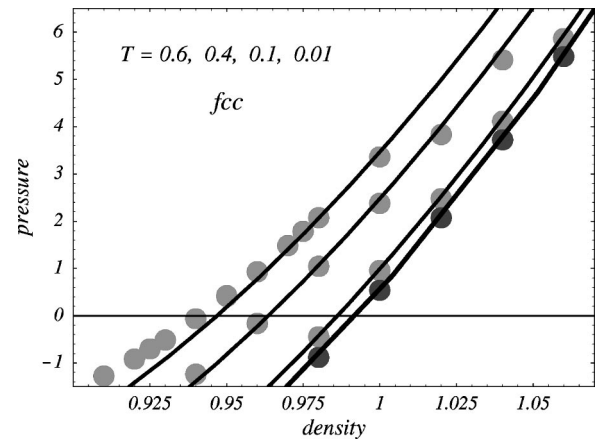


FIG. 5. The pressure in the fcc solid state, as a function of the density for the temperatures $T = 0.6, 0.4, 0.1, 0.01$ (from left to right). The dots mark the results from the MD calculation, and the curves stem from theoretical expressions explained in the text. All physical quantities are in standard LJ units.

to internal attraction. The theoretical pressure isotherms shown as curves are explained in the next subsection.

D. Equation of state

A modification of the Carnahan-Starling (CS) equation of state [16] for hard spheres to particles with softer repulsive interaction has been suggested and tested successfully in [17]. The equation of state involves the second virial coefficient and an effective volume v_{eff} , to be defined below, which also depends on the temperature. For potentials with attraction, an augmented van der Waals approximation has been proposed and tested for the LJ fluid [18]. A similar approach is used here. The potential contribution to the pressure of the fluid is a sum of the modified CS expression, involving an effective volume $v_{\text{eff}}(T)$, and terms associated with the attractive part of the interaction, $p^{\text{pot}}=p^{\text{rep}}+p^{\text{att}}$, with

$$p^{\text{rep}}=n k_B T \left(\frac{n B_2^{\text{rep}}}{(1-n v_{\text{eff}})^2} + 2 \frac{(n v_{\text{eff}})^2}{(1-n v_{\text{eff}})^3} \right), \quad (4)$$

$$p^{\text{att}}=n^2 k_B T (B_2 - B_2^{\text{rep}}) [1 + c(n, T)]. \quad (5)$$

Here B_2^{rep} is the second virial coefficient evaluated according to Eq. (2), but with the repulsive part ϕ^{rep} of the SHRAT potential only, i.e., the potential is cut off at its minimum and shifted such that it vanishes at $r/r_0=9/8$. For comparison, the repulsive part of the LJ potential is the WCA potential. The second virial coefficient calculated with the full SHRAT potential is denoted by B_2 . The correction $c(n, T)$, needed at higher densities, is presented later. The effective volume $v_{\text{eff}}(T)$ is given by $v_{\text{eff}}(T)=(\pi/6)d_{\text{eff}}^3$, with the effective diameter $d_{\text{eff}}=d_{\text{eff}}(T)$ determined by the distance where the repulsive part ϕ^{rep} of the binary interaction potential equals the thermal energy: $\phi^{\text{rep}}(d_{\text{eff}})=k_B T$. At the temperature $T=T_{\text{ref}}$, one has $d_{\text{ref}}=r_0$ and consequently $v_{\text{eff}}=(\pi/6)r_0^3 \approx 0.5236r_0^3$ for both the LJ and the SHRAT interactions. In the following, we use the relatively simple LJ expression $v_{\text{eff}}(T)=(\pi/6)r_0^3 \{2/[1+(k_B T/\Phi_0)^{1/2}]\}^{1/2}$ for the determination of the effective volume.

The dashed curves shown in Fig. 4 are the equations of state where only the repulsive part of the interaction has been taken into account. The thick and thin full curves correspond to the augmented van der Waals approximation with $c=0$ and

$$c=(3n v_{\text{eff}}+6n^2 v_{\text{eff}}^2) \exp(-\Phi_0/k_B T),$$

respectively. This expression, which fits the MD data quite well, is based on an educated guess rather than on a proper derivation. The temperature and the density at the critical point, as inferred from this equation of state, are $T_c/T_{\text{ref}}=0.794$ and $n_c/n_{\text{ref}}=0.32$. The pressure at the critical point is $p_c/p_{\text{ref}}=0.0097 \approx 0.01$. The compressibility factor $Z=p/(nk_B T)$ at the critical point is $Z_c \approx 0.38$, very close to the value $3/8=0.375$ following from the original van der Waals equation. For comparison, the last number is slightly

smaller, viz., ≈ 0.35 , for the LJ fluid. For simple gases like argon or nitrogen one has $Z_c \approx 0.31$.

A word of caution is in order. For the present system with the rather short-range attractive force, the triple point is rather close to the critical point. No attempt is made here to determine the complete phase behavior. However, there is a finite range of temperatures where one has a solid (at high densities), an at least metastable liquid (at intermediate densities), and a gas (at small densities), all at zero pressure. Physical systems where the liquid phase is only metastable are fluids composed of C_{60} and some colloidal solutions [19].

The curves shown in Fig. 5 stem from a modification of the pressure $p_{\text{cold}}(n)$ for particles placed on ideal fcc lattice sites. More specifically, the pressure in the solid phase p_{solid} is computed according to

$$p_{\text{solid}}(n, T) = n k_B T + \frac{1}{2} p_{\text{cold}}(n + s(n, T)) + \frac{1}{2} p_{\text{cold}}(n - s(n, T)), \quad (6)$$

where $s(n, T)=(2k_B T/e_2)^{1/2}$ with $s(n, 0)=0$, and $e_2=\partial^2 e_{\text{cold}}/\partial n^2$ is a density difference that takes into account that at finite temperatures the particles can approach each other more closely and can be further apart than at $T=0$. For temperatures below $T/T_{\text{ref}}=0.5$, the expression given above provides a reasonable approximation for the pressure in the solid phase.

IV. ELASTICITY COEFFICIENTS

The elastic properties of an effectively isotropic solid are characterized by the (isothermal) bulk modulus or compression modulus $B=n(\partial p/\partial n)_T$ and by the shear modulus G . The Born-Green expression [20] for this quantity, used in MD simulations, is the time average of a two-particle quantity, viz.,

$$G^{\text{BG}}=\frac{1}{15V} \left\langle \sum_{i<j} (r^{-2}(r^4 \phi')')^{ij} \right\rangle, \quad (7)$$

where the prime denotes the derivative with respect to r . This high frequency shear modulus is also nonzero in the fluid state [21]. Sometimes it is referred to as the Maxwell shear modulus. The low frequency shear modulus G , which is nonzero in the solid state but vanishes in the fluid state, is computed according to $G=G^{\text{BG}}+G^{\text{fluct}}$ [22,23]. The (negative) fluctuation contribution G^{fluct} involves a time average of the square of a two-particle quantity; thus it contains three- and four-particle contributions. For further details of the expressions used in the MD computations see, e.g., [17] and [24], where elasticity coefficients are presented for the WCA potential.

In cubic systems, the anisotropy of the shear modulus is reflected by the fact that one needs two coefficients to characterize the shear behavior. These can, e.g., be the largest and smallest values (for fcc and bcc) c_{44} (in Voigt notation)

and $\tilde{c}_{44} = (c_{11} - c_{12})/2$. The modulus c_{44} is associated with a displacement and its gradient parallel to the 100 and 010 directions. The shear modulus \tilde{c}_{44} pertains to a deformation where the displacement and its gradient enclose an angle of 45° with the 100 and 010 directions. The expressions used for the computation of the Born-Green and fluctuation contributions of c_{44} are

$$V c_{44}^{\text{BG}} = \left\langle \sum_{i < j} \left(\frac{1}{2} (x^2 + y^2) r^{-1} \phi' \right)^{ij} \right\rangle + \left\langle \sum_{i < j} (x^2 y^2 r^{-1} (r^{-1} \phi')')^{ij} \right\rangle, \quad (8)$$

and

$$V c_{44}^{\text{fluct}} = - \frac{1}{k_B T} [\langle C_{44}^2 \rangle - \langle C_{44} \rangle^2],$$

with

$$C_{44} \equiv \sum_{i < j} (x y r^{-1} \phi')^{ij}. \quad (9)$$

For \tilde{c}_{44} one uses similar expressions with xy replaced by $(x^2 - y^2)/2$. A measure for the anisotropy of the shear modulus is the ratio $c_{\text{anis}} = c_{44}/\tilde{c}_{44}$. For an effectively isotropic solid one has $c_{\text{anis}} = 1$; for many monocrystalline cubic (fcc and bcc) substances one finds values between 2 and 4, but both smaller and larger values also occur.

Alternatively, one describes the shear behavior of a cubic solid by the orientationally averaged shear modulus $G = (3c_{44} + 2\tilde{c}_{44})/5$ and the ‘‘cubic’’ modulus $G_c = \tilde{c}_{44} - c_{44}$. The bulk modulus of a cubic system is linked with the Voigt elasticity coefficients by $B = (c_{11} + 2c_{12})/3$. Just like the shear moduli, the isothermal bulk modulus is the sum of a Born-Green and a (negative) fluctuation contribution, $B = B^{\text{BG}} + B^{\text{fluct}}$ with $B^{\text{BG}} = 5G^{\text{BG}}/3 + 2p^{\text{pot}}$, and

$$V B^{\text{fluct}} = - \frac{1}{9 k_B T} [\langle B^2 \rangle - \langle B \rangle^2]$$

with

$$B \equiv \sum_{i < j} (r \phi')^{ij}. \quad (10)$$

Frequently the elastic behavior of an effectively isotropic solid is also characterized by the Young elasticity modulus E and the Poisson ratio ν . These quantities are linked with the bulk modulus and the orientationally averaged shear modulus G by $E = 9BG/(3B + G)$ and $\nu = (1/2)(3B - 2G)/(3B + G)$. In the fluid state one has $G = 0$ and consequently $E = 0$ and $\nu = 0.5$. For two-particle interactions, zero temperature, and zero pressure the Cauchy relation $B = 5G/3$ applies. Then one has $E = 5G/2$ and $\nu = 0.25$. Solid argon has the somewhat larger Poisson ratio 0.30. At low temperatures,

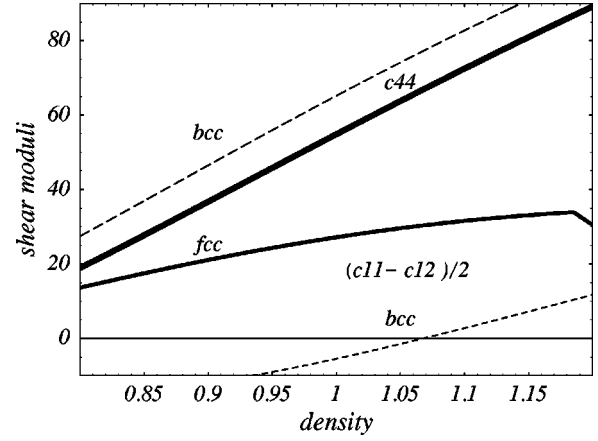


FIG. 6. The shear moduli c_{44} and $(c_{11} - c_{12})/2$ as functions of the density for ideal fcc and bcc lattices. All physical quantities are in standard LJ units.

one has $\nu = 0.27$ for iron and nickel, and $\nu = 0.22$ for silicon. Rather large and small values are $\nu = 0.41$ for gold and $\nu = 0.07$ for diamond.

For low temperatures, the elasticity coefficients can be inferred from the change of the energy when the ideal lattice is subjected to the appropriate deformation. Alternatively, one may use the Born-Green expression involving the first and second derivatives of the potential to compute the coefficients in the undistorted state.

Results of such calculations, here performed using MATHEMATICATM, are presented in Figs. 6 and 7. More specifically, the cold shear moduli c_{44} , \tilde{c}_{44} , E , and G are displayed as functions of the density for fcc (solid curves) and bcc (dashed curves) solids. Notice that $\tilde{c}_{44} = (c_{11} - c_{12})/2$ is negative for the bcc case when the density is smaller than $n/n_{\text{ref}} \approx 1.07$. Thus the bcc crystal not only has a larger energy than the fcc crystal (cf. Fig. 3), but it is also mechanically unstable for densities $n < 1.07n_{\text{ref}}$. The kink seen in the fcc curves is due to the contributions from the second coordination shell starting at the density $n/n_{\text{ref}} = 1.185$. For a less

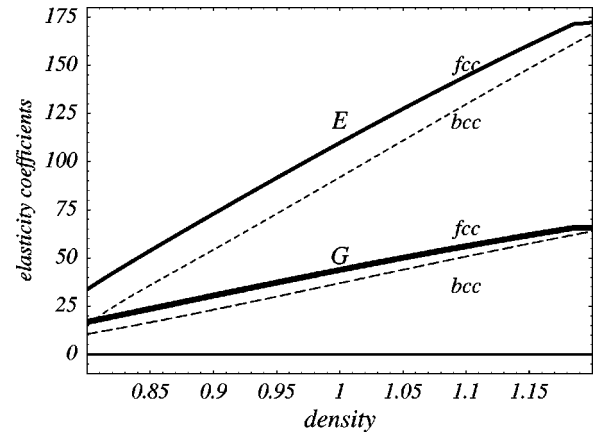


FIG. 7. The orientationally averaged shear modulus G and the elastic modulus E as functions of the density for particles placed on ideal fcc and bcc lattice sites. All physical quantities are in standard LJ units.

TABLE I. The isothermal bulk modulus B and three shear moduli, all in units of the reference pressure p_{ref} , as computed in the MD simulation. The superscript BG refers to the Born-Green expression for the shear moduli.

B	c_{44}	G	G_c	c_{44}^{BG}	G^{BG}	G_c^{BG}
44.8 ± 0.5	35.8 ± 0.3	28.6 ± 0.2	-18.2 ± 0.2	41.0 ± 0.1	32.9 ± 0.1	-20.2 ± 0.1

smooth cutoff such as, e.g., that used in the case of the WCA potential, one would have a jump at such a point.

The values for elasticity coefficients as inferred from MD simulations for the solid at the temperature $T/T_{\text{ref}}=0.6$ and the density $n/n_{\text{ref}}=0.942$ are given in Table I, in units of p_{ref} . At this state point, the average potential energy per particle e^{pot} and the pressure are $e^{\text{pot}}/\Phi_0 = -4.950$, $p/p_{\text{ref}} = 0.02$. The value of the shear modulus c_{44} as inferred from G and G_c according to $c_{44} = G - 2G_c/5$ agrees with the directly extracted value within the computational uncertainty. The same applies to the Born-Green contributions to these quantities. For the shear modulus \tilde{c}_{44} one infers from $\tilde{c}_{44} = G + 3G_c/5$ the value 17.7 ± 0.3 , in units of p_{ref} . The resulting anisotropy coefficient is $c_{\text{anis}} = c_{44}/\tilde{c}_{44} \approx 2.0$. The elastic modulus E and the Poisson ratio ν as computed from the values for B and G given in Table I are $E \approx 71$, in units of p_{ref} , and $\nu \approx 0.24$. The ratio G/B is ≈ 0.64 .

V. VISCOELASTIC AND PLASTIC BEHAVIOR

A. Remarks on nonequilibrium molecular dynamics simulations

Nonequilibrium molecular dynamics has been developed and applied to various problems during the last three decades; for books on this subject see [11–14]. In order to demonstrate that the model system exhibits typical liquidlike and solidlike behavior, examples of viscoelastic behavior in the liquid and of elastic and plastic behavior in the solid are presented next.

Here, we consider a simple shear flow in the x direction with the gradient of the velocity \mathbf{v} in the y direction. The shear rate $\dot{\gamma}$ is given by $\dot{\gamma} = \partial v_x / \partial y$. Such a flow can be generated either by moving boundaries or forces [25–27], or as here, by moving image particles undergoing an ideal Couette flow with the prescribed shear rate (homogeneous shear). Let the flow be switched on at $t=0$. Then at time t the image particles above (below) the basic (central) box have moved in the x direction to the right (left) by the distance $\dot{\gamma}tL$ modulo(L), where L is the length of the periodicity box in the y direction. Of course, the periodic boundary conditions for the particles leaving and entering the basic box have to be modified (Lees-Edwards boundary conditions, [28]). For a system in a fluid state in equilibrium and for not too large shear rates, a linear velocity profile typical for a plane Couette flow is set up in the basic box (from which the data are extracted). At high shear rates where pluglike flow also occurs it is essential to use a velocity “profile unbiased thermostat” (PUT, [29,27,30]). A shear flow can also be generated by modifying the equations of motion (Slid, so named because of its close relationship to the Dolls tensor algorithm

[11–13]). For reviews of NEMD results for rheological properties of simple and complex fluids, see [31–33].

Rheological properties such as the (non-Newtonian) viscosity and the normal pressure differences are obtained from the Cartesian components of the stress tensor $\sigma_{\mu\nu} = -p_{\mu\nu}$ or of the pressure tensor $p_{\mu\nu}$ which is the sum of kinetic and potential contributions $p_{\mu\nu} = p_{\mu\nu}^{\text{kin}} + p_{\mu\nu}^{\text{pot}}$,

$$Vp_{\mu\nu}^{\text{kin}} = \left\langle \sum_i m c_{\mu}^i c_{\nu}^i \right\rangle, \quad Vp_{\mu\nu}^{\text{pot}} = \frac{1}{2} \left\langle \sum_{ij} r_{\mu}^{ij} F_{\nu}^{ij} \right\rangle. \quad (11)$$

Here \mathbf{c}^i is the specific velocity of particle i , i.e., its velocity relative to the flow velocity $\mathbf{v}(\mathbf{r}^i)$, $\mathbf{r}^{ij} = \mathbf{r}^i - \mathbf{r}^j$ is the relative position vector of particles i, j , and \mathbf{F}^{ij} is the force acting between them. As before, the greek subscripts μ, ν , which assume the values 1,2,3, stand for Cartesian components associated with the x, y, z directions. In the simulations, the expression for the pressure tensor is averaged over many (10^3 to 10^6) time steps. For the present flow geometry, the (non-Newtonian) viscosity η is obtained by dividing the long time average of the $yx(21)$ component of the stress or pressure tensor by the shear rate: $\eta = \sigma_{yx} / \dot{\gamma} = -p_{yx} / \dot{\gamma}$.

From the simulation, the kinetic and potential contributions to the pressure tensor and to the viscosity can be computed separately. Only the sum can be measured in a real experiment. The kinetic contribution to the viscosity dominates in dilute gases [34]. In dense fluids (liquids) the potential contribution is more important.

Normal stress or pressure differences, e.g., $\sigma_{xx} - \sigma_{yy} = p_{yy} - p_{xx}$, have also been computed. At small shear rates one finds $-p_{yx} \sim \dot{\gamma}$ and $p_{yy} - p_{xx} \sim \dot{\gamma}^2$, as well as $p_{xx} + p_{yy} - 2p_{zz} \sim \dot{\gamma}^2$.

B. Viscoelastic behavior of the liquid

The viscoelastic behavior of a fluid is revealed by the growth of the shear stress in response to a shear deformation $\gamma = \dot{\gamma}t$ that is switched on at $t=0$. In Fig. 8, the shear stress $\sigma = \sigma_{xy}$ is shown as a function of the time for the shear rates $\dot{\gamma}/\dot{\gamma}_{\text{ref}} = 0.173, 0.346$ (bottom graph) and $0.87, 1.73$ (upper graph) for a liquid. The reference value for the shear rate is $\dot{\gamma}_{\text{ref}} = 1/t_{\text{ref}}$ with $t_{\text{ref}} = r_0/v_{\text{ref}}$ where $v_{\text{ref}} = (\Phi_0/m)^{1/2}$ is a reference velocity. The temperature and the density are $T/T_{\text{ref}} = 0.6$ and $n/n_{\text{ref}} = 0.725$, respectively. The dashed lines through the origin indicate the short-time behavior $\sigma = G_M \dot{\gamma}t$ with the Maxwell shear modulus G_M equal to the Born-Green value $G^{\text{BG}} = 15p_{\text{ref}}$ as inferred from the MD simulation. The full curves are the solution $\sigma = \eta \dot{\gamma} (1 - \exp(-t/\tau_M))$ of the Maxwell model with the (shear rate de-

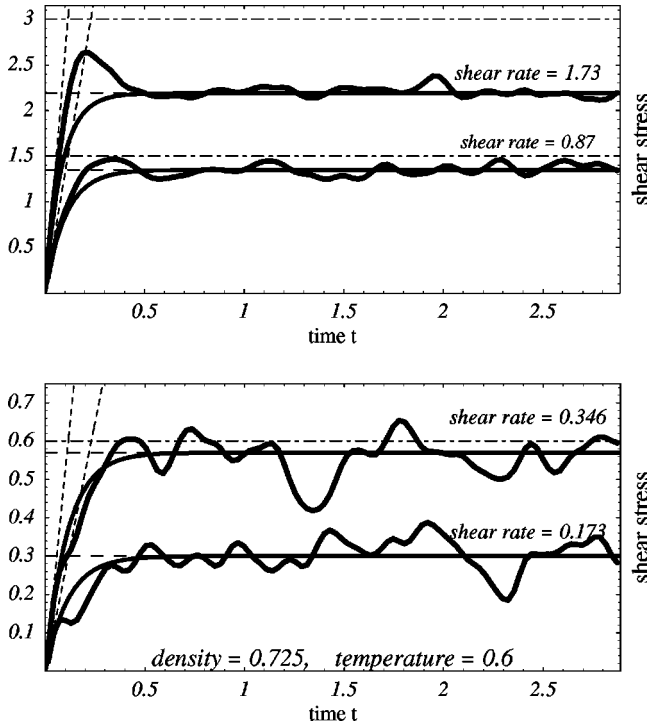


FIG. 8. The shear stress in the liquid phase as a function of the time, for four shear rates. The (full) curves correspond to solutions of the Maxwell model. The dashed lines through the origin mark the short-time elastic behavior. All physical quantities are in standard LJ units.

pendent) Maxwell relaxation time $\tau_M = \eta/G_M$. The values for the viscosity are $\eta/\eta_{\text{ref}} = 1.73, 1.64, 1.56, 1.26$, in increasing order of the shear rate. The reference viscosity is $\eta_{\text{ref}} = p_{\text{ref}} t_{\text{ref}}$. The dashed horizontal lines indicate the values the shear stress would approach if the (non-Newtonian) viscosity η , as inferred from the long-time average ($t \gg \tau_M$), did not decrease with increasing shear rate. The stress overshoot seen for the highest shear rate still stays below this limit. For reason of completeness, the full stationary non-Newtonian shear viscosity as a function of the shear rate as obtained in NEMD simulations for $T/T_{\text{ref}} = 1$ and $n/n_{\text{ref}} = 0.75$, as well as its kinetic and potential contributions, are shown in Fig. 9. Shear thinning is seen for shear rates $\dot{\gamma}/\dot{\gamma}_{\text{ref}} > 1$. The values for the zero rate viscosity at the state point studied are $\eta_{\text{kin}}/\eta_{\text{ref}} = 0.12 \pm 0.01$, $\eta_{\text{pot}}/\eta_{\text{ref}} = 1.50 \pm 0.07$, and $\eta/\eta_{\text{ref}} = 1.61 \pm 0.08$. The corresponding values computed in an (adiabatic) equilibrium simulation (at the same density, with an average temperature $T/T_{\text{ref}} = 0.99$) from integrals over the relevant time correlation functions are $\eta_{\text{kin}}/\eta_{\text{ref}} = 0.10 \pm 0.02$, $\eta_{\text{pot}}/\eta_{\text{ref}} = 1.48 \pm 0.09$, and $\eta/\eta_{\text{ref}} = 1.58 \pm 0.11$. There is good agreement within the computational uncertainty. The dashed curves above and below the line for the kinetic contribution (see Fig. 9) indicate the statistical uncertainty of the viscosity which, for small shear rates, increases proportionally to $\dot{\gamma}^{-1/2}$ when the averaging time t_{av} over which the data are extracted is chosen, as usual, as $t_{\text{av}} = C/\dot{\gamma}$, with a constant $C \geq 20$ was used. For the other two viscosities, the corresponding curves are not dis-

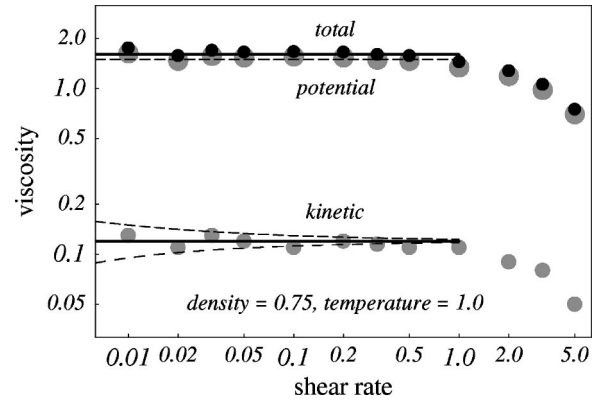


FIG. 9. Shear viscosity as a function of the shear rate as obtained in NEMD simulations for $T/T_{\text{ref}} = 1$ and $n/n_{\text{ref}} = 0.75$. The small and large gray dots mark the kinetic and potential contributions to the viscosity and the black dots represent their sum, viz., the “total” shear viscosity. Shear thinning is seen for shear rates $\dot{\gamma}/\dot{\gamma}_{\text{ref}} > 1$. The (solid and dashed) horizontal lines indicate the averages of the data points for $\dot{\gamma}/\dot{\gamma}_{\text{ref}} \leq 1$. The meaning of the other curves is explained in the text.

played since they could hardly be seen on the scale of the figure. For comparison, some values for the viscosity of the LJ liquid (with cutoff distance $r = 2.5$) at some similar state points, all for $T/T_{\text{ref}} = 1$, as found in the literature, are mentioned. In particular, in Ref. [35] for the two densities $n/n_{\text{ref}} = 0.70$ (0.84) the following extrapolated viscosities were obtained: $\eta_{\text{kin}}/\eta_{\text{ref}} = 0.16 \pm 0.06$ (0.10 ± 0.03), $\eta_{\text{pot}}/\eta_{\text{ref}} = 1.1 \pm 0.1$ (2.5 ± 0.1), and $\eta/\eta_{\text{ref}} = 1.26 \pm 0.16$ (2.6 ± 0.13). By evaluating a Green-Kubo formula for the comparable density $n/n_{\text{ref}} = 0.72$, the viscosity values $\eta/\eta_{\text{ref}} = 1.3 \pm 0.10$, and $\eta/\eta_{\text{ref}} = 1.25 \pm 0.13$ were reported in Refs. [36] and [37], respectively. These data, together with the value for the shear rate $\dot{\gamma}_{\text{onset}}$ at onset of shear thinning $\dot{\gamma}_{\text{onset}} \approx \dot{\gamma}_{\text{ref}}$ extracted from the data in Ref. [35] for the LJ fluid, reveal that the SHRAT fluid exhibits both a zero rate shear viscosity and shear rheological properties very close to the ones obtained for the LJ fluid. The shear thinning is associated with structural changes in the fluid that have been analyzed previously for other model substances [38].

C. Plastic flow of the solid

The elastic response and the plastic yielding of a solid at the temperature $T/T_{\text{ref}} = 0.6$ and the density $n/n_{\text{ref}} = 0.942$, where the pressure is approximately zero, are presented in Fig. 10. More specifically, the shear stress is plotted as a function of the time for a linearly growing displacement with the shear rate $\dot{\gamma}/\dot{\gamma}_{\text{ref}} = 0.001$. The thick and thin curves that stay close to each other correspond to isothermal simulations where one starts from an “aged” equilibrium state and from particles placed on ideal fcc lattice sites, respectively. The full and the dashed straight lines through the origin describe the elastic behavior with the full shear modulus c_{44} (labeled G) and the Born-Green contribution (labeled BG) to this modulus. The curve where the yield point occurs later, at a deformation $\gamma \approx 0.15$ rather than 0.12, also pertains to a star-

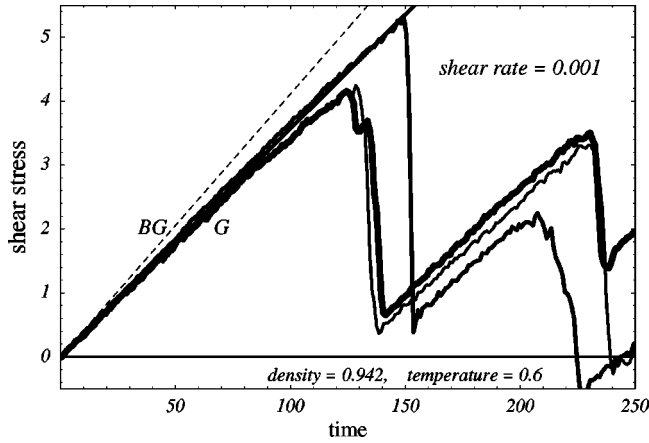


FIG. 10. The shear stress, in the solid phase, as a function of the time for the shear rate $\dot{\gamma}/\dot{\gamma}_{\text{ref}}=0.001$. All physical quantities are in standard LJ units.

tup from an ideal lattice but now to an adiabatic rather than an isothermal simulation. Notice that the elastic behavior as seen in Fig. 10 lasts about 1000 times longer than that of the liquid shown in Fig. 8.

For small shear rates, the elastic behavior and the occurrence of the yield point are approximately independent of the shear rate. The plastic flow behavior beyond this point, however, does depend on $\dot{\gamma}$. This is shown in Fig. 11 where the shear stress is displayed as a function of the time for the shear rates $\dot{\gamma}/\dot{\gamma}_{\text{ref}}=0.001, 0.002, 0.005$. The start is from an aged equilibrium state. In all cases the end times are chosen such that one has a shear deformation $\gamma=1.0$. At the smallest rate one observes a pronounced stick-slip flow; at higher shear rates a more continuous plastic flow occurs. The effective viscosity inferred from the long-time average of shear stress (or about one-half the maximum stress at the yield point) divided by the shear rate is several hundred times larger than the viscosities in the liquid state.

The stick-slip behavior, seen at the smallest shear rate, shows eight maxima of the shear stress over a shear deformation $\gamma=1$. The periodicity box contains 2×8 layers of particles; the displacement between opposite sides of the box is $\gamma_{\text{box}}=8\gamma$. Slips obviously occur when γ_{box} exceeds 1. Thus the eightfold repetition seems to be associated with the size of the system. The initial yielding at deformations just above 0.10, however, occurs for all shear rates shown. The latter phenomenon is an intrinsic property of the solid, and it may be expected in view of the Lindemann criterion which says that a crystal will melt when the displacement of atoms exceeds about one-tenth of the lattice constant. Of course, it is desirable to study the plastic flow at longer times and to analyze the structural changes. This, however, is outside the scope of the present article.

VI. SCALING AND REFERENCE VALUES

When one wants to compare properties as computed here with those of real materials, one has to specify the param-

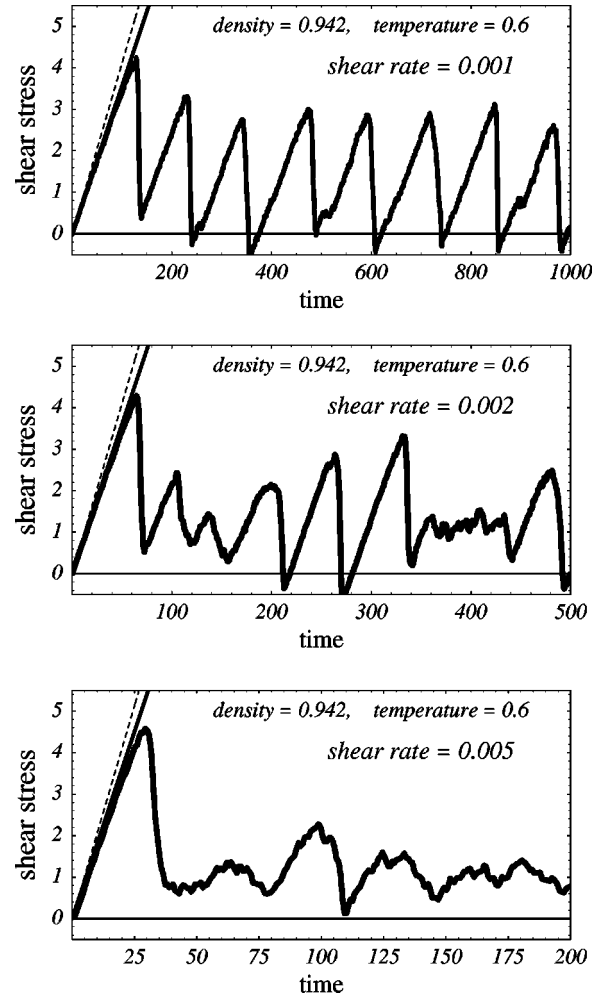


FIG. 11. The shear stress, in the solid phase, as a function of the time for the shear rates $\dot{\gamma}=0.001, 0.002, 0.005$. All physical quantities are in standard LJ units.

eters of the interaction potential, viz., the well depth Φ_0 , the characteristic length r_0 , and the mass m of the particles. It is stressed again that we do not want to mimic a particular substance but to provide a feeling for the order of magnitude of the reference quantities for various cases of interest. As an estimate for Φ_0 and r_0 one can use one-sixth of the binding energy e_b of an atom and the inverse of the third root of the number density, respectively, in the low temperature solid. Three sets of values are presented in Table II. The first one is the familiar argonlike substance, referred to as Ar. The second one is a substance composed of C_{60} molecules where values for the well depth and for r_0 were proposed in [19], although for a different, but also short-range, potential. The third set, referred to as SM, for standard material, is copper-like since the values for the characteristic energy, distance, and mass are chosen to match those of copper. As far as the orders of magnitude are concerned these values are typical for many solid materials one can touch every day. The coinage metals like silver, copper, gold, iron, and nickel have rather similar binding energies and interparticle distances, viz., 3.0, 3.5, 3.8, 4.3, 4.4 eV and 0.26, 0.23, 0.26, 0.23, 0.22 nm,

TABLE II. The characteristic reference values needed to convert the dimensionless variables used in the calculations to physical quantities for argon-, C_{60} -, and copperlike (the ‘‘standard material’’) substances.

Substance	e_b (eV)	r_0 (nm)	mass (10^{-27} kg)	T_{ref} (K)	n_{ref} (nm^{-3})	p_{ref} (10^6 Pa)	v_{ref} (m/s)	t_{ref} (10^{-12} s)	$\dot{\gamma}_{\text{ref}}$ (10^9 s $^{-1}$)	η_{ref} (10^{-3} Pa s)
Ar	0.08	0.34	66.7	160	25.4	40.7	182	18.7	53.5	0.76
C_{60}	1.66	0.96	1202	3200	1.13	36.4	19.2	49.9	20.0	1.81
SM	3.5	0.23	106	6800	82.2	5590	941	2.45	410	13.7

respectively. The values for germanium and silicon are not much different, viz., 3.9,4.6 eV and 0.28,0.27 nm. Of course, a true modeling of these materials requires more complicated potential functions, and is therefore not considered in this work. As input for Table II we used either the binding energy e_b or the temperature $T_{\text{ref}} = \Phi_0/k_B = e_b/(6k_B)$ associated with the potential well depth, either the diameter r_0 or the number density $n_{\text{ref}} = r_0^{-3}$, and the mass m . The derived reference quantities which are listed in Table II are p_{ref} for the pressure, the stress, and the elasticity coefficients, v_{ref} and t_{ref} for the velocity and the time, as well as $\dot{\gamma}_{\text{ref}}$ and η_{ref} for the shear rate and the viscosity.

VII. CONCLUDING REMARKS

In this article, a simple polynomial SHRAT potential has been introduced. It has a repulsive core, an attractive part, and is rather short ranged. The cutoff is smooth, such that the first and second derivatives vanish at the cutoff distance. These cooperative features produce considerable advantages in numerical studies; they enable efficient simulation studies of a model material that exhibits similarities to a full (but computationally expensive) LJ potential. The thermophysical properties of the model were calculated by MD and NEMD computer simulations. From a study of the pressure as a function of the density for various temperatures, the (co)existence of gaseous, metastable liquid, and solid (fcc) phases was found. Equations of state that fit the simulation data in certain regions of densities and temperatures were given. The elasticity coefficients and bulk and shear moduli, were determined both from MD and, for low temperature solids, by analytic lattice calculations. Particular attention was paid to the response of the system to an imposed shear deformation, switched on and proceeding with a constant shear rate. In the liquid state, typical viscoelastic behavior was observed, which can be described with a Maxwell model. The solid shows elastic behavior for small deformations. Beyond a critical deformation, the solid yields and undergoes a transition to plastic flow. At extremely small shear rates, the motion is of stick-slip type; at larger shear rates it is more continuous. Some examples were given for possible choices of the relevant model parameters and for the reference values needed to convert the dimensionless quantities used in the calculations to physical ones. The measured stationary shear viscosities for the SHRAT fluid compare very well with data previously reported for the LJ potential (cutoff at $r=2.5$).

The SHRAT potential is suitable for further studies of equilibrium and nonequilibrium properties. In particular, the

long-time behavior of the solid undergoing plastic flow and the accompanying structural changes should be analyzed. A comparison of the present model material with a metal modeled by the embedded atom method is desirable.

Colloidal dispersions can be looked upon as macrofluids and solids. With appropriate modifications, the present calculations could be applied to dispersions composed of spherical particles. The potential parameters could be guessed by the same method as used successfully in [39] to correlate results obtained from systems with screened Coulomb and with soft sphere interactions. A comparison with experimental data on shear deformation and plastic flow in colloidal crystals [40] should be rewarding.

Furthermore, the extension of the present approach to fluids composed of nonspherical particles is desirable. Liquid crystals can be treated by using the ideas of Gay and Berne [41,42] or of [43]. By introducing additional binding forces between the particles, one models chain molecules and treats polymeric liquids. As well as using LJ potentials to bind nearest neighbors along polymeric chains [44], it has become standard to use the WCA potential [45] or also a truncated LJ potential [46] as the interaction between all particles in the fluid and to combine it with a ‘‘finitely extensible nonlinear elastic’’ (FENE) potential [45] of the type $-(1/2)k\Phi_0(h/r_0)^2 \ln(1-r^2/h^2)$ for $r < h$ in order to model the interaction between every two adjacent monomers in a chain molecule. Here the quantity k is a spring coefficient, frequently chosen as $k=30$ for polymer melts, together with $h=1.5r_0$ for the cutoff distance and the maximum extension of a bond. Instead of the WCA potential, we propose to combine the present SHRAT potential with the FENE potential, with $k=20$ and $h=1.5r_0$. Compared with the potentials formerly applied to computations for polymers, this modeling has the advantage that states at zero pressure can be studied. Yet the computational advantages of the short range of the potential remain. It is expected that the liquid phase will be broader in the macromolecular systems than in the case considered here since crystallization becomes more difficult. On the other hand, the liquid state will have to compete with the glassy state.

ACKNOWLEDGMENTS

This work has been conducted under the auspices of the collaborative research projects SFB 448 ‘‘Mesoskopisch strukturierte Verbundsysteme’’ and SFB 605 ‘‘Elementarereignisse,’’ financially supported by the Deutsche Forschungsgemeinschaft (DFG).

- [1] G. Mie, *Ann. Phys. (Leipzig)* **11**, 657 (1903); E. Grüneisen, *ibid.* **26**, 393 (1908).
- [2] J.E. Lennard-Jones, *Physica (Amsterdam)* **4**, 941 (1937).
- [3] J.D. Weeks, D. Chandler, and H.C. Andersen, *J. Chem. Phys.* **54**, 5237 (1971).
- [4] B.D. Holian and D.J. Evans, *J. Chem. Phys.* **78**, 5147 (1983).
- [5] S. Hess, in *Computational Physics*, edited by K.H. Hoffmann and M. Schreiber (Springer, Berlin, 1996), p. 268.
- [6] W.G. Hoover and H.A. Posch, *Phys. Rev. E* **49**, 1913 (1994).
- [7] S. Hess and M. Kröger, *Phys. Rev. E* **61**, 4629 (2000).
- [8] H.H. Rugh, *Phys. Rev. Lett.* **78**, 772 (1997); O.G. Jepps, G. Ayton, and D.J. Evans, *Phys. Rev. E* **62**, 4757 (2000).
- [9] W.G. Hoover and S. Hess, *Physica A* **267**, 98 (1999).
- [10] S. Hess and M. Kröger, *Z. Angew. Math.* **80**, Suppl. 1, 49 (2000).
- [11] W.G. Hoover, *Molecular Dynamics* (Springer, Berlin, 1986); *Computational Statistical Mechanics* (Elsevier, Amsterdam, 1991); *Physica A* **194**, 450 (1993).
- [12] M.P. Allen and D.J. Tildesley, *Computer Simulation of Liquids* (Clarendon, Oxford, 1987).
- [13] D.J. Evans and G.P. Morriss, *Statistical Mechanics of Non-equilibrium Liquids* (Academic Press, London, 1990).
- [14] R. Haberlandt, S. Fritzsche, G. Peinel, and K. Heinzinger, *Molekular-Dynamik* (Vieweg, Braunschweig, 1995).
- [15] G.S. Grest, B. Dünweg, and K. Kremer, *Comput. Phys. Commun.* **55**, 269 (1989).
- [16] F. Carnahan and K.E. Starling, *J. Chem. Phys.* **51**, 635 (1969).
- [17] S. Hess, M. Kröger, and H. Voigt, *Physica A* **250**, 58 (1998).
- [18] S. Hess, *Physica A* **267**, 58 (1999).
- [19] M.H.J. Hagen, E.J. Meijer, G.C.A.M. Mooij, D. Frenkel, and H.N.W. Lekkerkerker, *Nature (London)* **365**, 425 (1993).
- [20] M. Born, *J. Chem. Phys.* **7**, 591 (1939); *Proc. Cambridge Philos. Soc.* **36**, 160 (1940); H.S. Green, *The Molecular Theory of Fluids* (North-Holland, Amsterdam, 1952); M.S. Green, *J. Chem. Phys.* **22**, 398 (1954).
- [21] R. Zwanzig and R.D. Mountain, *J. Chem. Phys.* **43**, 4464 (1965).
- [22] D.R. Squire, A.C. Holt, and W.G. Hoover, *Physica (Amsterdam)* **42**, 388 (1969); W.G. Hoover, A.C. Holt, and D.R. Squire, *ibid.* **44**, 437 (1969).
- [23] M. Schoen, S. Hess, and D.J. Diestler, *Phys. Rev. E* **52**, 2587 (1995).
- [24] S. Hess, M. Kröger, and W.G. Hoover, *Physica A* **239**, 449 (1997).
- [25] W.T. Ashurst and W.G. Hoover, *Phys. Rev. Lett.* **31**, 206 (1972); *Phys. Rev. A* **11**, 658 (1975); W.G. Hoover and W.T. Ashurst, *Theor. Chem. Adv. Persp.* **1**, 331 (1975).
- [26] E.M. Gosling, I.R. McDonald, and K. Singer, *Mol. Phys.* **26**, 1475 (1973).
- [27] S. Hess and W. Loose, *Physica A* **162**, 138 (1989).
- [28] A.W. Lees and S.F. Edwards, *J. Phys. C* **5**, 1921 (1972).
- [29] W.G. Hoover, *Annu. Rev. Phys. Chem.* **34**, 103 (1983); D.J. Evans and G.P. Morriss, *Comput. Phys. Rep.* **1**, 287 (1984); D.J. Evans and W.G. Hoover, *Annu. Rev. Fluid Mech.* **18**, 243 (1986).
- [30] W. Loose and S. Hess, *Rheol. Acta* **28**, 91 (1989); in *Microscopic Simulation of Complex Flows*, Vol. 292 of *NATO Advanced Study Institute, Series E: Applied Sciences*, edited by M. Mareschal (Plenum Press, New York, 1990); S. Hess and W. Loose, *Ber. Bunsenges. Phys. Chem.* **94**, 216 (1990).
- [31] S. Hess, M. Kröger, W. Loose, C. Pereira Borgmeyer, R. Schramek, H. Voigt, and T. Weider, in *Monte Carlo and Molecular Dynamics of Condensed Matter Systems*, edited by K. Binder and G. Ciccotti, *IPS Conf. Proc. Vol. 49* (IPS, Bologna, 1996), p. 825.
- [32] S. Hess, C. Aust, L. Bennett, M. Kröger, C. Pereira Borgmeyer, and T. Weider, *Physica A* **240**, 126 (1997).
- [33] S. Hess, in *Advances in the Computer Simulations of Liquid Crystals*, Vol. 545 of *NATO Advanced Study Institute, Series C: Mathematical and Physical Sciences*, edited by P. Pasini and C. Zannoni, (Kluwer, Dordrecht, 2000), p. 189.
- [34] W. Loose and S. Hess, *Phys. Rev. Lett.* **58**, 2443 (1988); *Phys. Rev. A* **37**, 2099 (1988).
- [35] S. Hess, in *Vielteilchen-Systeme*, Vol. 5 of *Bergmann Schaefer Lehrbuch der Experimentalphysik*, edited by W. Raith (Walter de Gruyter, Berlin, 1992), pp. 227–292.
- [36] M. Schoen and C. Hoheisel, *Mol. Phys.* **56**, 653 (1985).
- [37] D.M. Heyes, *J. Chem. Soc., Faraday Trans. 2* **79**, 1741 (1983).
- [38] S. Hess and H.J.M. Hanley, *Phys. Lett.* **98A**, 35 (1983); H.J.M. Hanley, J.C. Rainwater, and S. Hess, *Phys. Rev. A* **36**, 1795 (1987); J.C. Rainwater, H.J.M. Hanley, and S. Hess, *Phys. Lett. A* **136**, 450 (1988).
- [39] S. Hess, J.B. Hayter, and R. Pynn, *Mol. Phys.* **53**, 1527 (1984).
- [40] D.A. Weitz, W.D. Dozier, and P.M. Chaikin, *J. Phys. (Paris), Colloq.* **46**, C3-257 (1985); H.M. Lindsay and P.M. Chaikin, *ibid.* **46**, C3-269 (1985).
- [41] J.B. Gay and B.J. Berne, *J. Chem. Phys.* **74**, 3316 (1981).
- [42] D.J. Adams, G.R. Luckhurst, and R.W. Phippen, *Mol. Phys.* **61**, 1575 (1987); E. de Miguel, L.F. Rull, M.K. Chalam, and K.E. Gubbins, *ibid.* **71**, 1223 (1991); **72**, 593 (1991); **74**, 405 (1991); E. de Miguel, E. Martin del Rio, J.T. Brown, and M.P. Allen, *J. Chem. Phys.* **105**, 4234 (1996); E. de Miguel and E. Martin del Rio, *Phys. Rev. E* **55**, 2916 (1997).
- [43] S. Hess and Bin Su, *Z. Naturforsch. A: Phys. Sci.* **54**, 559 (1999).
- [44] S. Hess, *J. Non-Newtonian Fluid Mech.* **23**, 305 (1987).
- [45] H.R. Warner, *Ind. Eng. Chem. Fundam.* **11**, 379 (1972); K. Kremer and G.S. Grest, *J. Chem. Phys.* **92**, 5057 (1990); M. Kröger, W. Loose, and S. Hess, *J. Rheol.* **37**, 1057 (1993); J. Gao and J.H. Weiner, *Macromolecules* **27**, 1201 (1994); F. Affouard, M. Kröger, and S. Hess, *Phys. Rev. E* **54**, 5178 (1996); M. Kröger and R. Makhloufi, *ibid.* **53**, 2531 (1996).
- [46] A.R.C. Baljon and M.O. Robbins (unpublished).